Neuron

NeuroResource

A genetically encoded fluorescent sensor for monitoring spatiotemporal prostaglandin E2 dynamics *in vivo*

Graphical abstract

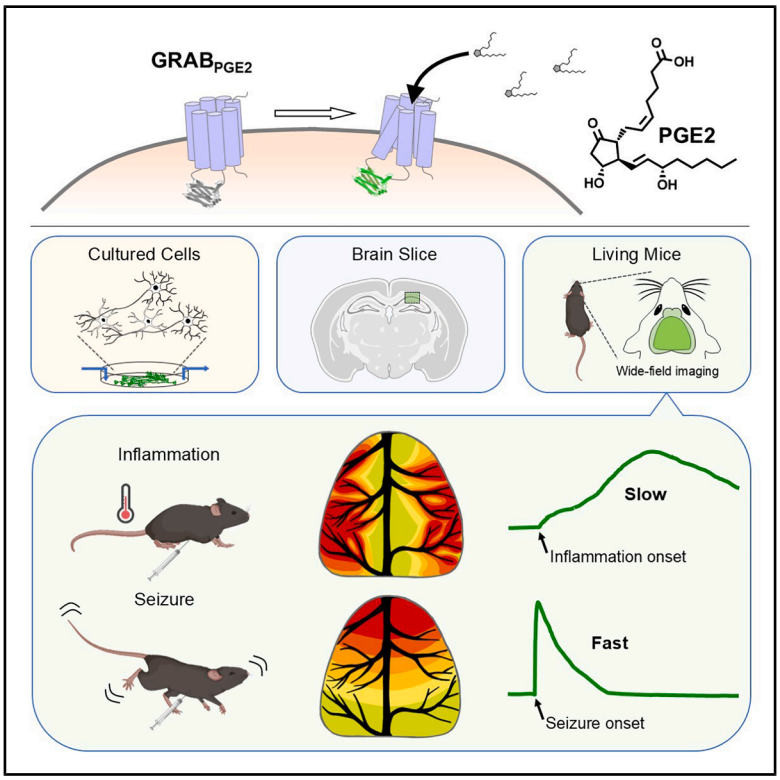

Highlights

- GRAB$_{PGE2}$ is a genetically encoded GPCR activation-based sensor for PGE2
- GRAB$_{PGE2-1.0}$ can detect PGE2 with high specificity and spatiotemporal resolution
- GRAB$_{PGE2-1.0}$ enables real-time detection of endogenous PGE2 dynamics *in vivo*
- GRAB$_{PGE2-1.0}$ reveals distinct patterns of PGE2 during inflammation versus seizure

Authors

Lei Wang (王蕾), Yini Yang (杨旖旎), Fei Deng (邓飞), ..., Bohan Li (李柏翰), Jinxia Wan (万金霞), Yulong Li (李毓龙)

Correspondence

yulongli@pku.edu.cn

In brief

Wang et al. develop a genetically encoded fluorescent sensor for prostaglandin E2 (PGE2). This sensor, GRAB$_{PGE2-1.0}$, can specifically detect real-time extracellular PGE2 dynamics in cultured cells, acute brain slices, and living mice. By applying the GRAB$_{PGE2-1.0}$ sensor, the authors reveal distinct temporal and spatial patterns of cortical PGE2 during inflammation versus seizures.

Wang et al., 2026, Neuron *114*, 1–13
June 3, 2026
https://doi.org/10.1016/j.neuron.2026.01.030

CellPress

Neuron

CellPress

NeuroResource

A genetically encoded fluorescent sensor for monitoring spatiotemporal prostaglandin E2 dynamics *in vivo*

Lei Wang (王蕾),[1,2,3,6] Yini Yang (杨旖旎),[2,3,6] Fei Deng (邓飞),[2,3] Yuqi Yan (鄢羽岐),[2,3,4] Huan Wang (王欢),[2,3] Bohan Li (李柏翰),[2,4] Jinxia Wan (万金霞),[2,3] and Yulong Li (李毓龙)[1,2,3,4,5,7,*]

[1]Peking University, Tsinghua University, National Institute of Biological Sciences Joint Graduate Program, Peking University, Beijing 100871, China

[2]State Key Laboratory of Membrane Biology, Peking University School of Life Sciences, Beijing 100871, China

[3]PKU-IDG/McGovern Institute for Brain Research, Beijing 100871, China

[4]Peking-Tsinghua Center for Life Sciences, New Cornerstone Science Laboratory, Academy for Advanced Interdisciplinary Studies, Peking University, Beijing 100871, China

[5]National Biomedical Imaging Center, Peking University, Beijing 100871, China

[6]These authors contribute equally

[7]Lead contact

*Correspondence: yulongli@pku.edu.cn

https://doi.org/10.1016/j.neuron.2026.01.030

SUMMARY

Prostaglandin E2 (PGE2) is an important lipid signaling molecule that regulates a wide range of physiological and pathological processes. However, its dynamics during these processes are largely unknown due to the lack of tools to directly visualize PGE2 with high spatiotemporal resolution. Here, we developed and characterized a genetically encoded G-protein-coupled receptor (GPCR) activation-based (GRAB) PGE2 sensor, which we call $GRAB_{PGE2\text{-}1.0}$ (PGE2-1.0), that has high specificity for PGE2, nanomolar affinity, rapid kinetics, and high spatial resolution when expressed both *in vitro* and *in vivo*. Using fiber-photometry recordings, we found that PGE2-1.0 can reliably monitor endogenous PGE2 dynamics in the preoptic area in the brain during acute inflammation. Wide-field *in vivo* imaging with PGE2-1.0 reveals spatial heterogeneity in cortex-wide PGE2 dynamics during acute inflammation and seizure. Thus, our PGE2-1.0 sensor can be used to detect endogenous PGE2 dynamics with high spatiotemporal resolution, providing a robust tool for studying PGE2 under specific physiological and pathological conditions.

INTRODUCTION

Prostaglandins play an important role in regulating a variety of physiological and pathological processes. Prostaglandin E2 (PGE2)—the most abundant prostaglandin in the human body—is produced by a wide range of cell types in a variety of organisms.[1,2] PGE2 is closely associated with the onset and progression of inflammation, pain, fever, and neurological diseases,[3] and inhibiting prostaglandin production has long been an important strategy for improving anti-inflammatory and analgesic treatments.[4,5] PGE2 is synthesized from arachidonic acid by the cyclooxygenase (COX) and prostaglandin E synthase (PTGES) enzyme families,[3,6,7] with COX enzymes serving as the key target for non-steroidal anti-inflammatory drugs (NSAIDs).[4] Inhibiting COX activity—particularly COX-2 activity—to reduce PGE2 production is a widely used clinical strategy to alleviate pain, inflammation, and fever.[4]

PGE2 exerts its biological functions primarily by binding to and activating its four receptors (EP1, EP2, EP3, and EP4), which are widely expressed throughout the central nervous system.[8–10] Importantly, the expression levels of these receptors differ across various brain regions,[8–10] and these receptors have different affinities for PGE2.[11] Thus, monitoring PGE2 dynamics will serve as an important step toward understanding the mechanisms underlying PGE2's various functions; however, the spatiotemporal dynamics of PGE2 remain largely unknown due to the lack of suitable tools for detecting PGE2 with high specificity, sensitivity, and spatiotemporal resolution. Unlike classic neurotransmitters stored in synaptic vesicles, evidence suggests that PGE2 is not stored within the cell but is synthesized and released on demand.[1,12] Hence, the expression levels of COX-2 and PTGES (particularly PTGES1) enzymes[6,13,14] are widely used as an indirect measure of PGE2 levels, as methods used to directly detect PGE2 lack sufficient spatiotemporal resolution. For example, measuring PGE2 usually requires the extraction of tissue or blood samples, followed by purification and analysis steps, including radioimmunoassay,[15] enzyme-linked immunosorbent assay,[16,17] chromatography, and mass

Please cite this article in press as: Wang et al., A genetically encoded fluorescent sensor for monitoring spatiotemporal prostaglandin E2 dynamics *in vivo*, Neuron (2026), https://doi.org/10.1016/j.neuron.2026.01.030

spectrometry.[18,19] Although this approach can provide precise information regarding PGE2 levels, it has poor spatiotemporal resolution and cannot be used for real-time recording *in vivo*. On the other hand, microdialysis can measure molecules in the brain with high specificity, but it is difficult to use to detect hydrophobic molecules such as PGE2 and has low spatial and temporal resolution (with a sampling interval typically ranging from 20 to 30 min).[20,21] Therefore, a genetically encoded tool to specifically detect PGE2 with high spatiotemporal resolution *in vivo* would fill a significant need in this field.

In recent years, many genetically encoded fluorescent sensors have been developed to visualize specific neurochemicals using minimally invasive methods and providing high spatiotemporal resolution. One highly successful example of this approach is the G-protein-coupled receptor (GPCR) activation-based (GRAB) strategy, in which a series of genetically encoded fluorescent sensors was developed based on various GPCRs and conformation-sensitive circularly permuted enhanced green fluorescent protein (cpEGFP), thus allowing the user to detect specific GPCR ligands such as neurotransmitters and neuromodulators with high specificity and high sensitivity.[22–28] Here, we used this strategy to develop a genetically encoded fluorescent sensor specific to PGE2. We found that this sensor, which we call $GRAB_{PGE2\text{-}1.0}$ (hereafter PGE2-1.0), has high specificity for PGE2, high sensitivity (with a peak change in fluorescence >1,000% in response to PGE2), rapid kinetics, and negligible coupling to downstream signaling. We then examined the *in vitro* performance of PGE2-1.0 expressed in cultured cells and acute mouse brain slices. Finally, we expressed PGE2-1.0 in the mouse brain and monitored extracellular PGE2 dynamics during both inflammation and seizure *in vivo*.

RESULTS

Development and characterization of a $GRAB_{PGE2}$ sensor

To measure PGE2 dynamics with high spatial and temporal resolution, we developed a genetically encoded GRAB sensor for PGE2 (Figure 1A) based on the GRAB strategy. First, we systematically searched for the most suitable GPCR scaffold from four known human PGE2 receptors, namely the EP1, EP2, EP3, and EP4 receptors. For each GPCR, the third intracellular loop (ICL3) was replaced with the cpEGFP-containing ICL3 derived from our previously well-characterized green fluorescent norepinephrine sensor $GRAB_{NE1m}$,[24] using various insertion sites. Candidate sensors were then screened for suitable membrane trafficking (Figures S1A–S1C) and change in fluorescence ($\Delta F/F_0$) in response to PGE2 (Figure S1D). After this initial screening, we identified a human EP2-based candidate as the prototype sensor, which we call PGE2-0.1 (Figure S1D). Next, to improve the sensor's response, we conducted three optimization steps: (1) fine-tuning the ICL3 insertion sites, (2) truncating the linker region between the EP2 scaffold and cpEGFP, and (3) introducing mutations in the linker region and critical residues in cpEGFP. After screening more than 2,000 variants, we identified PGE2-1.0 as the variant with the largest response (~700%) to 1 μM PGE2 (Figures 1B and S2). In addition, based on the human EP2 structure,[29] we performed a mutagenesis screen of eight amino acids located near the receptor's ligand-binding pocket and generated a PGE2-insensitive sensor (for use as a negative control) containing a single missense mutation ($T113^{2.54}W$) in PGE2-1.0. We call this ligand-insensitive sensor PGE2mut (Figure 1B).

When expressed in HEK293T cells, PGE2-1.0 traffics to the plasma membrane and produces a dose-dependent increase in fluorescence in response to extracellular PGE2 application. In addition, the sensor's mean (±standard error of the mean [SEM]) half-maximal effective concentration (EC_{50}) for PGE2 is 42 ± 10 nM, similar to the EC_{50} reported for the wild-type EP2 receptor.[11] By contrast, as expected, PGE2mut traffics to the plasma membrane but has no detectable response to PGE2 application, even at 10 μM (Figures 1C and 1D). With respect to ligand specificity, the PGE2-1.0 sensor has a considerably lower EC_{50} (i.e., higher affinity) for PGE2 compared with the structurally similar prostaglandins PGD2, PGF2α, and PGI2 (with EC_{50} values of 24 μM, 195 μM, and 1 mM, respectively) (Figure 1E). In addition, the PGE2-induced response was fully blocked by the EP2 receptor antagonist PF04418948, and no detectable response was induced by any other lipid molecules tested, such as docosahexaenoic acid (DHA) and sphingosine-1-phosphate (S1P), or by any classic neurotransmitters or neuromodulators tested (Figure 1E).

We also examined the sensor's spectral properties, kinetics, and possible downstream coupling in HEK293T cells. Using one-photon excitation, the excitation peak of PGE2-1.0 is ~500 nm with an isosbestic point at ~420 nm, and the emission peak is 520 nm. Using two-photon excitation, the excitation peak is ~920 nm (Figure 1F). Using local perfusion and high-speed line-scanning (Figure 1G), we measured rapid response kinetics, with an average on-rate (τ_{on}) of 0.4 s and an average off-rate (τ_{off}) of 2 s (Figure 1H). To detect whether the PGE2-1.0 sensor engages downstream signaling pathways, we used the luciferase complementation assay and the Tango assay to measure activation of the GPCR-mediated Gs and β-arrestin pathways, respectively. As expected, the wild-type EP2 receptor couples robustly to both pathways. By contrast, PGE2-1.0 has only negligible downstream coupling in response to PGE2 (Figures 1I and 1J), confirming that expressing and activating the sensor does not affect the cell's intrinsic signaling pathways.

To examine the performance of PGE2-1.0 when expressed in a physiologically relevant cell type, we expressed the sensor and the ligand-insensitive PGE2mut in cultured rat cortical neurons by infection with adeno-associated virus (AAV). We found that both PGE2-1.0 and PGE2mut are expressed widely throughout the plasma membrane, both on the cell body and on neurites (Figure 2A). Moreover, the PGE2-1.0 sensor had a robust dose-dependent fluorescence response to PGE2 application, with an EC_{50} of 66 ± 4 nM (Figures 2B and 2C). By contrast, PGE2mut produced no detectable response to PGE2 even at the highest concentration tested (Figure 2C). In addition, application of a saturating concentration of PGE2 led to a peak increase in PGE2-1.0 fluorescence of 1,400%, with no measurable response in neurons expressing PGE2mut (Figure 2D). Similar to our results obtained with HEK293T cells, PGE2-1.0 had high specificity for PGE2 when expressed in neurons (Figure 2E). Finally, PGE2-1.0 produced a highly stable fluorescence

Please cite this article in press as: Wang et al., A genetically encoded fluorescent sensor for monitoring spatiotemporal prostaglandin E2 dynamics *in vivo*, Neuron (2026), https://doi.org/10.1016/j.neuron.2026.01.030

CellPress

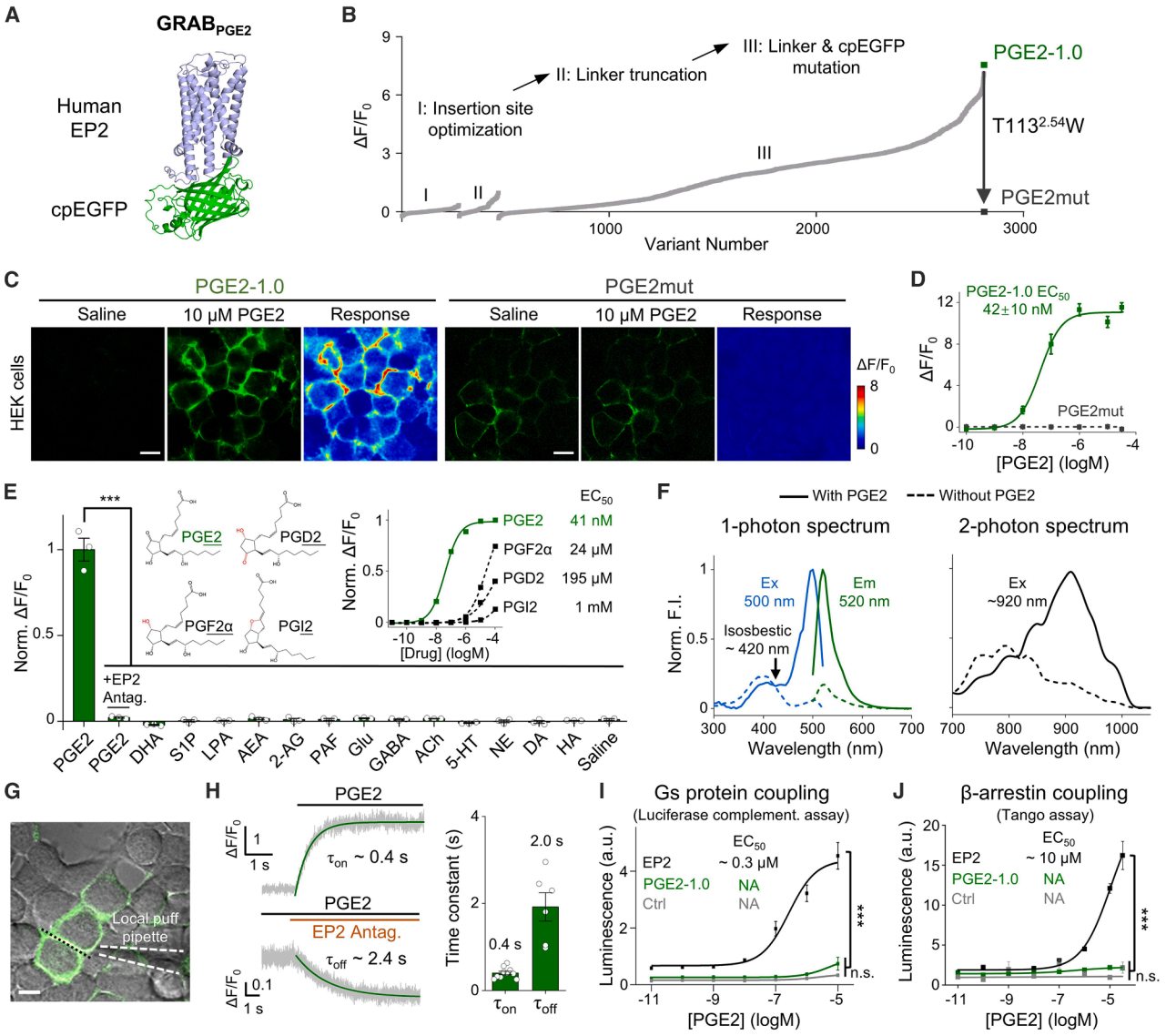

Figure 1. Development, optimization, and characterization of PGE2-1.0 in HEK293T cells

(A) Drawing depicting the structure of the GRAB$_{PGE2}$ sensor, consisting of the human EP2 receptor and cpEGFP.

(B) The steps used to screen and optimize candidate PGE2 sensors, resulting in PGE2-1.0, as well as the development of a ligand-insensitive PGE2mut to serve as a negative control.

(C) PGE2-1.0 and PGE2mut were expressed in HEK293T cells, and the change in fluorescence was measured in response to 10 μM PGE2. Scale bars, 20 μm.

(D) Dose-response curves for PGE2-1.0 and PGE2mut expressed in HEK293T cells.

(E) The left inset shows the structures of PGE2, PGD2, PGF2α, and PGI2, while the right inset shows the dose-response curves for PGE2-1.0 in response to these four prostaglandins. The main graph shows the normalized change in fluorescence in response to the indicated compounds (each applied at 1 μM, except the EP2 antagonist PF04418948, which was applied at 10 μM); *n* = 3 coverslips/group.

(F) The one-photon and two-photon spectra of the PGE2-1.0 sensor measured in the absence (dashed lines) or presence (solid lines) of 10 μM PGE2.

(G) The local puffing system, in which a glass pipette containing 10 μM PGE2 was positioned above a PGE2-1.0-expressing cell. The dotted black line indicates the region of interest (ROI) for line scanning. Scale bar, 20 μm.

(H) Left: a representative trace of the change in PGE2-1.0 fluorescence measured using line scanning upon application of 10 μM PGE2 (top) and 100 μM EP2 antagonist (bottom); the solid green lines indicate the exponential fit to the data. Right: summary of the on (*n* = 10 cells/3 coverslips) and off (*n* = 6 cells/3 coverslips) time constants (τ_{on} and τ_{off}, respectively).

(I) Luciferase complementation assay for assessing downstream coupling to Gs proteins. Ctrl, Gs-LgBit alone; *n* = 3 cultures each.

(J) Tango assay for assessing downstream coupling to β-arrestin. Ctrl, no receptor; *n* = 3 cultures each.

All summary data are presented as the mean ± the standard error of the mean (SEM). Data in (I) and (J) were analyzed using one-way ANOVA followed by Tukey's test for multiple comparisons. Where indicated, n.s., not significant ($p > 0.05$), ***$p < 0.001$.

Please cite this article in press as: Wang et al., A genetically encoded fluorescent sensor for monitoring spatiotemporal prostaglandin E2 dynamics *in vivo*, Neuron (2026), https://doi.org/10.1016/j.neuron.2026.01.030

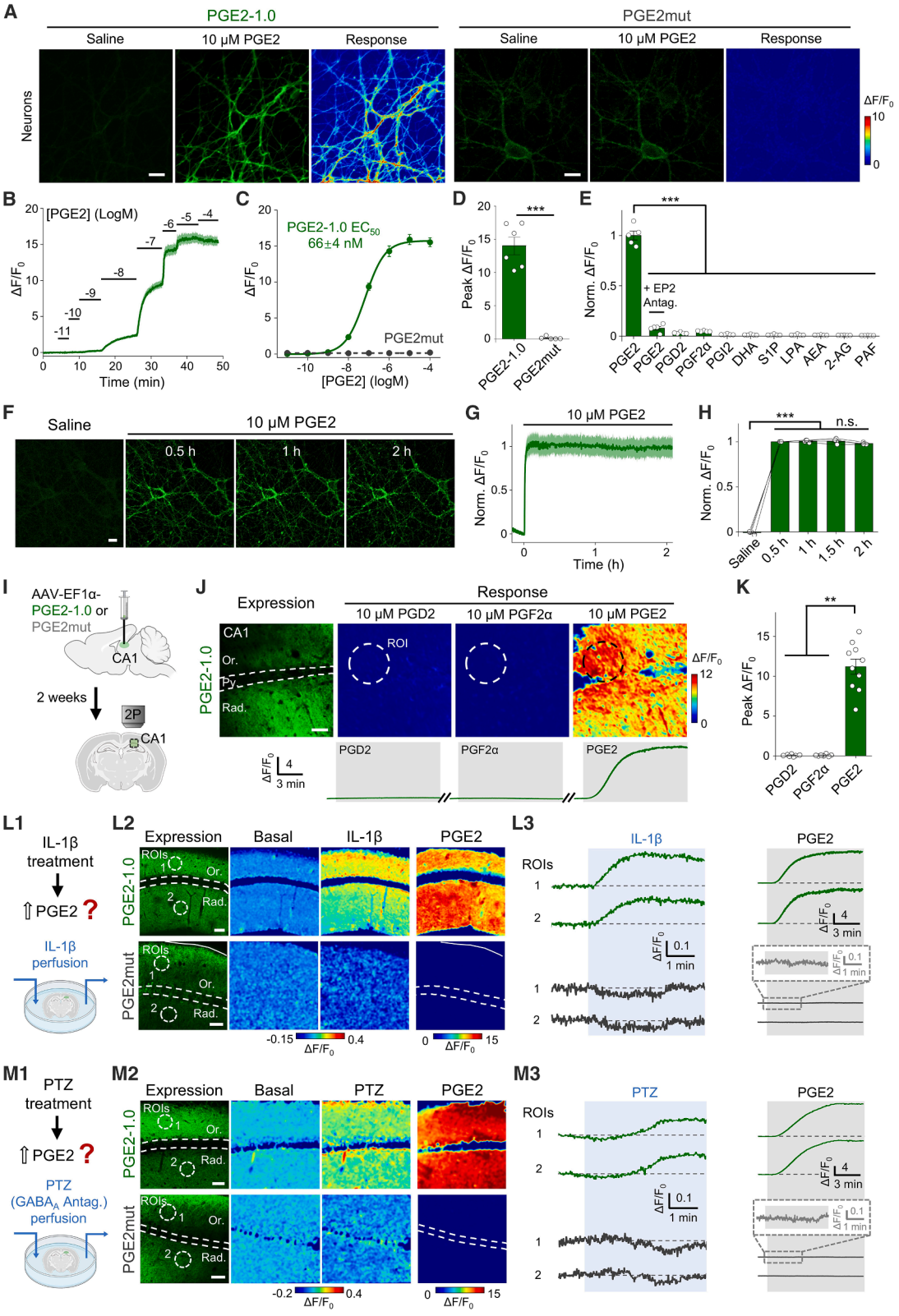

(legend on next page)

Please cite this article in press as: Wang et al., A genetically encoded fluorescent sensor for monitoring spatiotemporal prostaglandin E2 dynamics *in vivo*, Neuron (2026), https://doi.org/10.1016/j.neuron.2026.01.030

response for up to 2 h in the presence of 10 μM PGE2, indicating minimal sensor internalization or desensitization (Figures 2F–2H). Overall, these results confirm that our PGE2-1.0 sensor can be used to reliably measure PGE2 dynamics *in vitro* with high sensitivity, specificity, and spatiotemporal resolution.

PGE2-1.0 can be used to report endogenous PGE2 dynamics in acute brain slices

Next, we examined whether PGE2-1.0 can be used to monitor PGE2 dynamics in acute brain slices. We therefore injected AAV encoding PGE2-1.0 or PGE2mut in the hippocampal CA1 region of adult mouse brains. After 2 weeks (to allow for expression), we prepared acute brain slices and measured fluorescence in the CA1 region using two-photon microscopy (Figure 2I). We found that PGE2-1.0 responded specifically to PGE2, with an average peak response of ~1,100% when applied at 10 μM. By contrast, no response was measured for PGD2 or PGF2α (Figures 2J and 2K).

We then examined whether PGE2-1.0 can reliably detect changes in endogenous PGE2 in the hippocampal CA1 region. Given that PGE2 is closely related to inflammation,[4,30] we perfused the cytokine interleukin (IL)-1β (10 ng/mL) on the slices to mimic an inflammation-like condition and measured the change in fluorescence (Figure 2L1). We found that IL-1β induced a significant increase in PGE2-1.0 fluorescence in both the stratum oriens and stratum radiatum layers of the CA1. By contrast, PGE2mut was expressed at high levels but had no measurable response to either IL-1β or PGE2 application (Figures 2L and S3). Similarly, given the close relationship between PGE2 synthesis and synaptic activity, including seizure activity,[31] we applied the $GABA_A$ receptor antagonist pentylenetetrazol (PTZ) to mimic seizure-like activity (Figure 2M1). We found that PTZ induced a significant increase in PGE2-1.0 fluorescence, while PGE2mut had no measurable response to PTZ or PGE2 (Figures 2M and S3). Taken together, these results confirm that our PGE2-1.0 sensor can reliably measure changes in endogenous PGE2.

Detecting endogenous PGE2 dynamics *in vivo*

Based on our characterization of PGE2-1.0 in cultured cells and acute brain slices, we next asked whether this sensor can be used *in vivo* to detect endogenous PGE2 in the brain. PGE2 is known to mediate fever in the brain during inflammatory conditions.[3,4] Endogenous pyrogens and exogenous pyrogens such as lipopolysaccharide (LPS) can lead to an increase in PGE2 levels, which in turn can mediate hyperthermia or hypothermia (with high-dose pyrogens) via EP3 receptors in the preoptic area (POA).[32–35] Specifically, the median preoptic nucleus (MnPO) within the POA serves as the critical hub for this regulation, characterized by dense EP3 expression.[9,36] Moreover, inhibiting PGE2 synthesis or knocking out the enzymes involved in its synthesis (primarily PTGES1 and COX-2) in the MnPO was shown to effectively reduce pyrogen-induced fever.[20,33,37,38] Therefore, to test the ability of PGE2-1.0 to measure changes in endogenous PGE2 in the brain in response to pyrogens, we performed fiber-photometry recordings of PGE2-1.0 fluorescence specifically in this region while measuring body temperature in mice following LPS stimulation.

We first expressed PGE2-1.0 in the mouse brain by injecting the AAV into the MnPO, a subregion of the POA in the

Figure 2. Characterization of PGE2-1.0 expressed in cultured neurons and acute brain slices

(A) PGE2-1.0 and PGE2mut were expressed in primary cultured cortical neurons, and the change in fluorescence was measured in response to 10 μM PGE2. Scale bars, 20 μm.

(B) Example trace of the change in fluorescence in response to the indicated concentrations of PGE2 in primary cultured cortical neurons expressing PGE2-1.0, and the data represent 30 ROIs measured in 1 coverslip.

(C) Dose-response curve of PGE2-1.0 and PGE2mut in response to PGE2 measured in primary cultured cortical neurons.

(D) Summary of peak $\Delta F/F_0$ measured in neurons expressing PGE2-1.0 (n = 6 coverslips) or PGE2mut (n = 5 coverslips).

(E) Summary of the normalized change in PGE2-1.0 fluorescence measured in primary cultured cortical neurons in response to the indicated prostaglandins and lipids (each applied at 1 μM, except the EP2 antagonist, which was applied at 10 μM); n = 5 coverslips/group.

(F) Example images of cultured neurons expressing PGE2-1.0, showing the fluorescence change in response to a 2-h application of 10 μM PGE2; scale bar, 20 μm.

(G and H) Example trace (G) and summary (H) of the normalized change in PGE2-1.0 fluorescence in the continued presence of 10 μM PGE2; n = 4 coverslips.

(I) Schematic diagram depicting the strategy for injecting virus in the CA1 region of the mouse hippocampus, followed by fluorescence imaging of coronal slices using two-photon microscopy.

(J) Top: expression of PGE2-1.0 in the CA1 region, and pseudo-color images of PGE2-1.0 in response to PGD2, PGF2α, and PGE2. Scale bar, 50 μm. The dashed circles show the ROIs used to measure the change in fluorescence, and the layers in the CA1 region are indicated (Or, stratum oriens; Py, stratum pyramidale; Rad, stratum radiatum). Bottom: traces of PGE2-1.0 fluorescence measured in the ROIs shown above, before and after application of PGD2, PGF2α, and PGE2.

(K) Summary of the peak change in PGE2-1.0 fluorescence in response to PGD2 (n = 7 slices from 6 mice), PGF2α (n = 7/5), and PGE2 (n = 10/7) perfusion.

(L1) Schematic drawing depicting the strategy for measuring the effect of IL-1β (10 ng/mL) on PGE2 levels in brain slices expressing PGE2-1.0 or PGE2mut.

(L2) Expression and pseudo-color images of the change in PGE2-1.0 and PGE2mut fluorescence in acute brain slices. The dashed circles indicate the ROIs used in L3, and the layers in the CA1 region are indicated. Scale bars, 50 μm.

(L3) Example traces of the change in PGE2-1.0 and PGE2mut fluorescence in response to IL-1β (left) and PGE2 (right).

(M1) Schematic drawing depicting the strategy for measuring the effect of $GABA_A$ receptor antagonist pentylenetetrazol (PTZ, 15 mM) in brain slices expressing PGE2-1.0 or PGE2mut.

(M2) Expression and pseudo-color images of the change in PGE2-1.0 and PGE2mut fluorescence in acute brain slices. Scale bars, 50 μm.

(M3) Example traces of the change in PGE2-1.0 and PGE2mut fluorescence in response to PTZ (left) and PGE2 (right) application. Note the different pseudo-color scales for PGE2 in (L) and (M).

All summary data are presented as the mean ± SEM. Data in (D) were analyzed using Student's t test, and data in (E), (H), and (K) were analyzed using one-way ANOVA followed by Tukey's test for multiple comparisons. Where indicated, n.s., not significant ($p > 0.05$), $^{**}p < 0.01$, $^{***}p < 0.001$.

See also Figure S3.

Please cite this article in press as: Wang et al., A genetically encoded fluorescent sensor for monitoring spatiotemporal prostaglandin E2 dynamics *in vivo*, Neuron (2026), https://doi.org/10.1016/j.neuron.2026.01.030

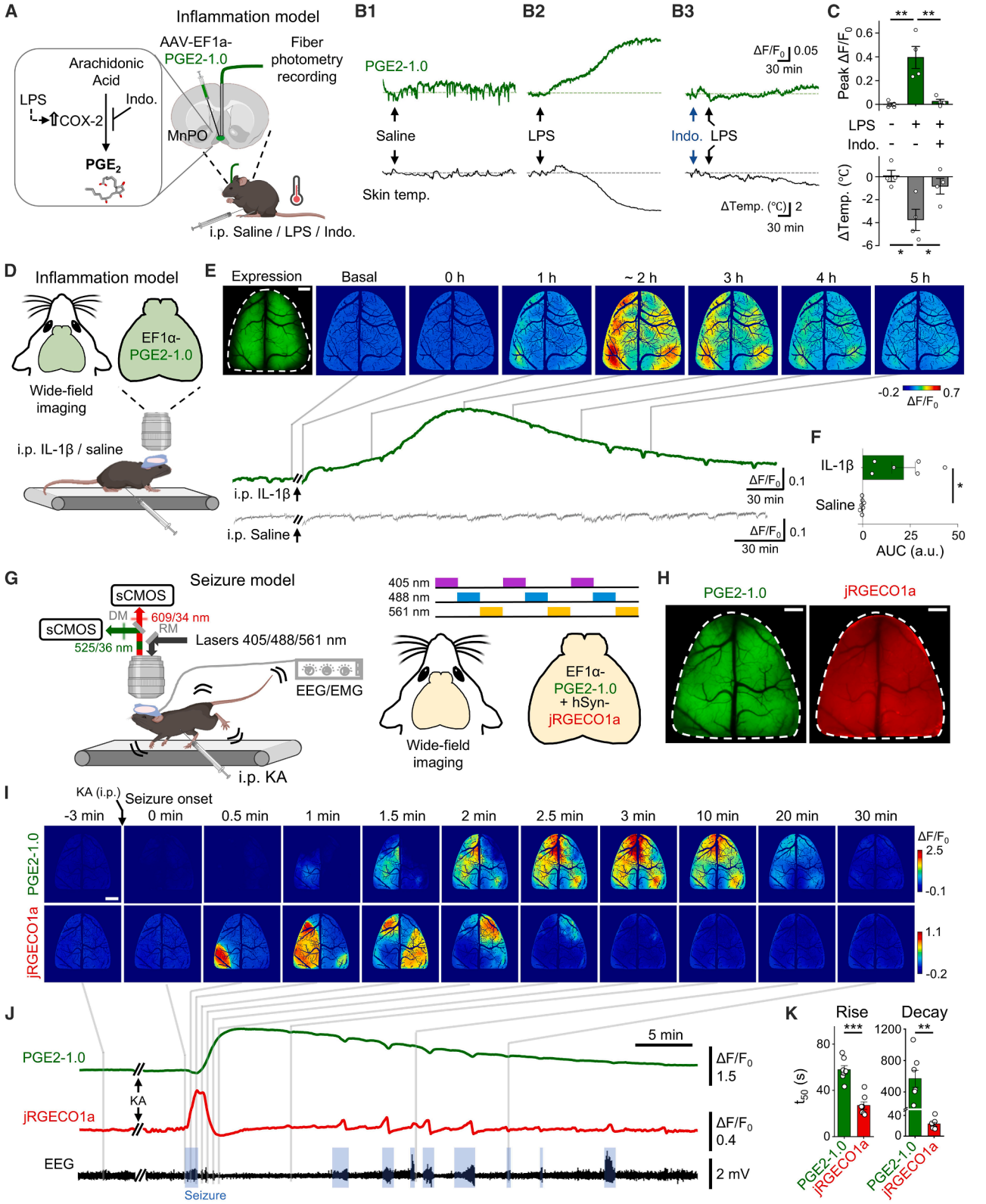

(legend on next page)

Please cite this article in press as: Wang et al., A genetically encoded fluorescent sensor for monitoring spatiotemporal prostaglandin E2 dynamics *in vivo*, Neuron (2026), https://doi.org/10.1016/j.neuron.2026.01.030

hypothalamus. We then implanted an optic fiber for subsequent recording (Figure 3A). We found that LPS (1 mg/kg body weight) induced a slow (over the course of 2–4 h) but steady increase in PGE2-1.0 fluorescence, together with a decrease in the mouse's skin temperature, indicating an increase in endogenous PGE2 levels in the MnPO (Figures 3B and 3C). To confirm the specificity of the PGE2-1.0 response, we pre-treated mice with the COX inhibitor indomethacin (Indo, 15 mg/kg body weight) 30 min prior to LPS administration and found that the LPS-induced PGE2-1.0 response and change in skin temperature were significantly reduced (Figures 3B and 3C). Thus, using this classic paradigm of LPS-induced acute inflammation, PGE2-1.0 has sufficient sensitivity and specificity to detect changes in endogenous PGE2 *in vivo*. Furthermore, our control experiments confirmed that the presence of the sensor does not affect the mouse body temperature response mediated by endogenous PGE2 (Figure S4).

Using PGE2-1.0 to monitor inflammation- and seizure-induced changes in cortical PGE2 with high spatiotemporal resolution

Although PGE2 and its receptors are widely distributed throughout the brain,[8–10] dynamic changes in PGE2 in specific brain regions are seldom studied due to the lack of suitable detection methods. Taking advantage of the PGE2-1.0 sensor's high specificity and spatiotemporal resolution, we expressed the sensor in the mouse cerebral cortex and then used mesoscopic imaging to measure endogenous PGE2 during various paradigms such as inflammation and seizure activity.

We first expressed the PGE2-1.0 sensor homogeneously throughout the cerebral cortex and then measured the change in fluorescence in response to an intraperitoneal (i.p.) injection of IL-1β (25 μg/kg body weight) or saline (Figure 3D). We found that IL-1β caused a gradual increase in PGE2-1.0 fluorescence that peaked at ∼22% above baseline and then slowly returned to baseline levels. By contrast, saline had no effect on PGE2-1.0 fluorescence (Figures 3E and 3F; Video S1). In contrast to the inflammation model, we observed no significant fluorescence changes in PGE2-1.0 during voluntary running events, comparable to the EGFP-CAAX control (Figure S5). This suggests that general physiological motor activity does not trigger a global or significant increase of cortical PGE2.

Next, we examined PGE2 dynamics in a kainic acid (KA)-induced seizure model. PGE2 has long been studied for its close connection with the onset and progression of seizure activity,[39–42] but little is currently known regarding the spatiotemporal changes in PGE2 levels during seizure, much less the relationship between PGE2 and other seizure-related signals such as calcium (Ca^{2+}). To address these questions, we co-expressed PGE2-1.0 and the red fluorescent Ca^{2+} sensor jRGECO1a[43] in the cerebral cortex. In addition, we implanted electroencephalography (EEG) and electromyography (EMG) electrodes to monitor seizure activity (Figure 3G). After allowing the mice to recover for 2 weeks, we used a custom-built wide-field microscope to record both PGE2-1.0 and jRGECO1a fluorescence together with the EEG and EMG signals (Figure 3G). Dual-color imaging confirmed that both PGE2-1.0 and jRGECO1a were expressed homogeneously throughout the dorsal cortex (Figure 3H). After allowing the mouse to adapt to the wide-field imaging device, we gave an i.p. injection of KA (10 mg/kg body weight). During seizure activity, we measured a transient increase in Ca^{2+} that started in a relatively small initial area and then rapidly spread to surrounding regions throughout the entire cortex. By contrast, the PGE2 signal did not propagate but increased gradually throughout the cortex over time after seizure onset (Figure 3I; Video S2), thus revealing a spatial pattern distinct from the Ca^{2+} signal. Detailed time-sequence visualization further highlights this distinction, clearly showing the rapid propagation of the Ca^{2+} wave and the generalized, gradual elevation of PGE2 (Figure S6A). Crucially, the PGE2-1.0 showed no response to saline injection, confirming the specificity of the observed PGE2 signals (Figures S6B–S6E). In addition, the

Figure 3. Using the PGE2-1.0 sensor to measure inflammation- and seizure-induced changes in PGE2 *in vivo*

(A) Left: diagram depicting the pathway for PGE2 synthesis and compounds that block or increase the activity of specific components in this pathway. LPS, lipopolysaccharide; COX-2, cyclooxygenase-2; Indo., indomethacin. Right: schematic diagram depicting the strategy for injecting virus, implanting optic fibers, and fiber-photometry recording in the MnPO region of the mouse brain, and the animal's skin temperature was also recorded during the experiment.

(B) Example traces of the change in PGE2-1.0 fluorescence and skin temperature in response to an i.p. injection of saline (B1), 1 mg/kg body weight LPS (B2), or 1 mg/kg body weight LPS following a pre-injection of 15 mg/kg body weight indomethacin (B3).

(C) Summary of the peak change in PGE2-1.0 fluorescence and skin temperature (n = 4 mice).

(D) Schematic diagram depicting the strategy used for wide-field imaging, and PGE2-1.0 was expressed throughout the cortical region, and the mice were head-fixed for wide-field imaging.

(E) Top: expression and pseudo-color images of the change in PGE2-1.0 fluorescence at the indicated times, and where indicated, IL-1β (25 μg/kg body weight) or saline was injected i.p. Scale bar, 1 mm. Bottom: corresponding example traces of PGE2-1.0 fluorescence.

(F) Summary of the area under the curve (AUC, in arbitrary units) of the change in PGE2-1.0 fluorescence measured for 240 min after injecting IL-1β (n = 6 mice) or saline (n = 7 mice).

(G) Schematic diagram depicting the strategy for dual-color wide-field imaging in a kainic acid (KA)-induced seizure model. sCMOS, scientific complementary metal oxide semiconductor camera; DM, dichroic mirror; RM, reflective mirror.

(H) Expression of PGE2-1.0 and jRGECO1a in the mouse cortex. Scale bars, 1 mm.

(I) Representative images of the change in PGE2-1.0 and jRGECO1a fluorescence in response to an i.p. injection of KA (10 mg/kg body weight). Scale bars, 1 mm.

(J) The representative traces of the change in PGE2-1.0 and jRGECO1a fluorescence, together with the corresponding EEG signal. The blue shaded boxes in the EEG trace indicate epileptic discharges.

(K) Summary of the rise and decay kinetics of the change in PGE2-1.0 and jRGECO1a fluorescence measured during seizure activity; n = 6 mice.

All summary data are presented as the mean ± SEM. Data in (C), (F), and (K) were analyzed using Student's t test. Where indicated, $^{*}p < 0.05$, $^{**}p < 0.01$, $^{***}p < 0.001$.

See also Figures S4 and S6.

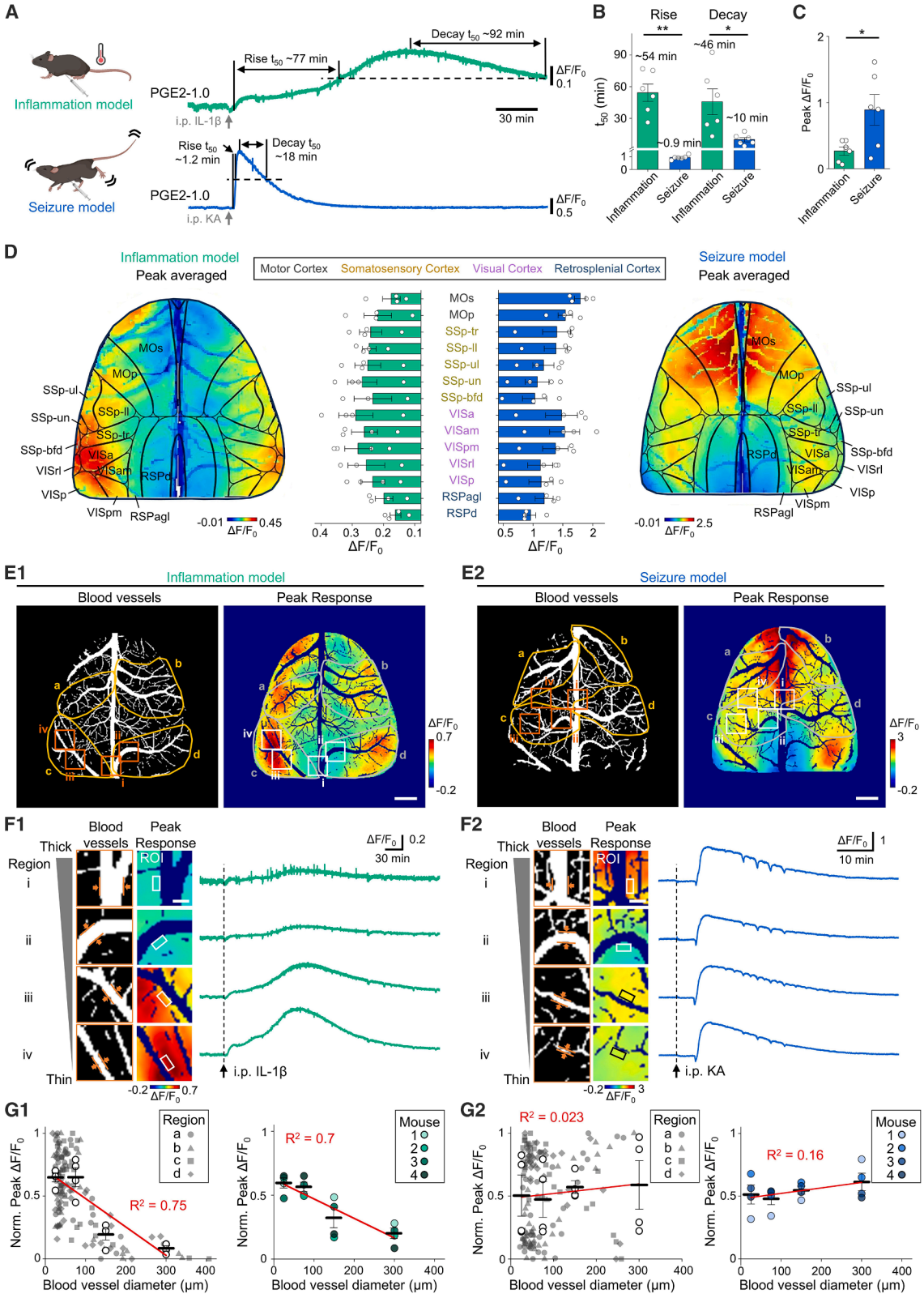

(legend on next page)

Please cite this article in press as: Wang et al., A genetically encoded fluorescent sensor for monitoring spatiotemporal prostaglandin E2 dynamics *in vivo*, Neuron (2026), https://doi.org/10.1016/j.neuron.2026.01.030

PGE2 and Ca^{2+} signals had distinct temporal features—immediately after seizure onset, we observed a rapid rise and fall in the Ca^{2+} signal, while the PGE2-1.0 signal began slightly later than the Ca^{2+} signal, increased relatively slower, and reached a maximum response of ~150% that was maintained for several minutes (Figures 3I, 3J, and S6A). To quantify this difference, we measured the rise and decay kinetics (t_{50}) of the PGE2 and Ca^{2+} signals and found that the PGE2 signal was significantly slower than the Ca^{2+} signal (Figure 3K). Thus, our results reveal significant differences in the spatiotemporal patterns of PGE2 and Ca^{2+} during seizure activity.

Interestingly, we also observed notable differences in the spatiotemporal dynamics of PGE2 between the inflammation and seizure models. First, in terms of the temporal dynamics, we found that both the rise and decay kinetics of PGE2 were significantly faster in the seizure model compared with the inflammation model (Figures 4A and 4B). Second, the average peak change in PGE2 during seizure was significantly larger compared with inflammation (Figures 4A and 4C). It is worth noting that although PGE2 has long been studied for its close connection with the onset and progression of seizures, it was previously considered to participate primarily in the chronic inflammation that accompanies seizures.[39–42] Thus, unlike traditional methods used to monitor PGE2, which are unable to capture rapid changes, the high temporal resolution of our PGE2-1.0 sensor makes it a robust new tool for detecting rapid changes in endogenous PGE2 levels.

With respect to the spatial patterns, we also found key differences between the two disease models, with notable differences in the location of the resulting signals. Specifically, the seizure-induced changes in PGE2 levels were largely observed in the anterior cortex, while the inflammation-induced changes in PGE2 did not appear to differ among various cortical subregions (Figure 4D). It is also worth noting that in all cortical subregions, the seizure-induced changes in PGE2 are significantly larger than inflammation-induced responses (Figure S7). In the acute inflammation model, the area with the largest response was relatively close to the peripheral regions of the cortex, near the ends or bifurcations of large blood vessels (Figure 4E1). By contrast, the area with the largest response in the seizure model was closer to anterior brain regions (Figure 4E2). An analysis of the correlation between the PGE2-1.0 response and the diameter of adjacent blood vessels revealed that the inflammation-induced change in PGE2 was relatively larger near small-diameter vessels (Figures 4F1 and 4G1). By contrast, we found no correlation between the seizure-induced change in PGE2 and the diameter of adjacent blood vessels (Figures 4F2 and 4G2). Together, these results indicate that our new PGE2-1.0 sensor has sufficient temporal and spatial resolution to reveal highly detailed information regarding the dynamic changes in PGE2 under physiological and pathological conditions.

DISCUSSION

Here, we report the development and characterization of a genetically encoded fluorescent sensor for detecting PGE2 with high specificity, rapid kinetics, and high spatiotemporal resolution. We also show that this sensor can be used to reliably monitor changes in endogenous PGE2 both *in vitro* and *in vivo*.

Using fiber photometry and mesoscopic imaging, we observed that PGE2 levels increase slowly following an i.p. injection of the pro-inflammatory agents LPS and IL-1β, reaching peak levels after 2–4 h. This is consistent with previous studies[20,32,34,44] and suggests that specific brain regions rely on similar—or closely related—mechanisms for the production and release of PGE2 in response to acute inflammation. In addition, we measured PGE2 during seizure activity and found a rapid increase (within ~2 min) in extracellular PGE2 levels following the onset of seizure. While previous studies focused primarily on the long-term increase in PGE2, for example, 24 h or several days after seizure, and examined the associated chronic inflammation,[31,42,45–48] our results demonstrate that robust changes in PGE2 levels begin much earlier after seizure onset. These distinct timescales of PGE2 elevation in inflammation versus seizure likely reflect different underlying mechanisms. The inflammation-induced response aligns with the well-known inducible COX-2-dependent pathway,[3,49] which requires *de novo* transcription and translation, leading to an intrinsic ≥1 h delay. By contrast, the rapid seizure-induced PGE2 increase occurs far faster (seconds to minutes) than inducible COX-2 could account for. Such kinetics suggest constitutive sources, potentially microglial COX-1,[50] which is

Figure 4. The PGE2-1.0 sensor reveals distinct temporal and spatial differences in PGE2 dynamics in the brain

(A) Schematic diagram depicting the IL-1β-induced inflammation and KA-induced seizure models (left), and representative traces of the change in PGE2-1.0 fluorescence in response to an i.p. injection of IL-1β or KA (right). In the traces, the rise and decay t_{50} values are indicated.

(B) Summary of the rise and decay t_{50} values for the change in PGE2 fluorescence measured as shown in (A); note the break in the *y* axis; $n = 6$ mice for each group, inflammation or seizure.

(C) Summary of the peak change in PGE2-1.0 fluorescence measured during inflammation and seizure; $n = 6$ mice.

(D) Pseudo-color images depicting the average peak increase in PGE2-1.0 fluorescence measured during inflammation (left) and seizure (right), and shown in the middle are the peak responses measured in the indicated cortical structures; $n = 4$ mice.

(E) Representative images of the cortical blood vessel structures (left) and the peak increase in PGE2-1.0 fluorescence (right) measured during inflammation (E1) and seizure (E2), and the ROIs used in (F) and (G) are indicated. Scale bars, 1 mm.

(F) Magnified views of the images of regions i–iv shown in (E) (left) and traces of the change in PGE2 fluorescence measured at the ROIs indicated by the rectangles (right). Scale bar, 200 μm.

(G) Left: normalized peak increase in PGE2-1.0 fluorescence plotted against the adjacent blood vessel diameter in the ROIs shown in (E) in the inflammation (G1) and seizure (G2) models, and each point represents the data from one single ROI. The correlation coefficients are also shown. Right: normalized peak increase in PGE2-1.0 fluorescence plotted against the adjacent blood vessel diameter for 4 mice, and also shown are the correlation coefficients.

All summary data are presented as the mean ± SEM. Data in (B) and (C) were analyzed using Student's *t* test. Where indicated, $^{*}p < 0.05$, $^{**}p < 0.01$.

See also Figure S7.

implicated in early illness-related responses,[51–53] or the basal, activity-regulated COX-2 present in discrete populations of neurons in the hippocampus and cortex.[31,54,55] Elucidating the source of this rapid PGE2 surge would be helpful for interpreting the efficacy of anti-inflammatory treatments and guiding future seizure research.

With respect to the spatial patterns of PGE2, we found notable differences in cortical PGE2 changes between the inflammation and seizure models. Specifically, acute inflammation induced a relatively large response close to the cortical periphery, near major blood vessel endings or bifurcations, while seizure induced the largest response near anterior brain regions (Figures 4E–4G). The blood vessels have long been recognized as an important source of PGE2 in response to the immune challenge.[38,56–59] Previous studies indicate that both COX-2 and PTGES1 are induced in brain endothelia cells during inflammation,[57,60,61] with a preference for small- to medium-sized vessels.[38] In addition, knocking out COX-2 or the terminal PGE2 synthase specifically in endothelial cells can abolish the LPS- and IL-1β-induced fever response.[38,59,62] Consistent with previous studies, the PGE2-1.0 provides a direct visualization of PGE2 dynamics, and the vascular-associated elevation of PGE2 we have observed during inflammation may reflect the conserved topological feature during neuroinflammation, further supporting the hypothesis that PGE2 originates in the vascular endothelium. By contrast, as discussed above, the major source of seizure-induced acute PGE2 elevation might be much different from the inflammation model, that being triggered directly or indirectly by excessive neuronal activities and leading to a distinct spatial pattern.

It is also worth noting that as a fluorescent protein-based sensor, PGE2-1.0 is subject to limitations common to this class of tools, such as potential sensitivity to motion artifacts, pH changes, or hemodynamic-related optical changes. Indeed, we observed small, transient decreases in our fluorescence signal that were temporally correlated with ictal events. We attribute these dips to artifacts, likely resulting from the robust seizure-induced hemodynamic changes (e.g., increased cerebral blood volume and vasodilation leading to light absorption and scattering) that are known to occur during ictal activity.

In summary, our genetically encoded PGE2-1.0 sensor can be used to reliably measure changes in endogenous PGE2 with high specificity, sensitivity, and spatiotemporal resolution, providing a robust new tool for studying PGE2 dynamics both *in vitro* and *in vivo*.

RESOURCE AVAILABILITY

Lead contact

Requests for further information, resources, and reagents should be directed to and will be fulfilled by the lead contact, Yulong Li (yulongli@pku.edu.cn).

Materials availability

Plasmids expressing the sensors used in this study were deposited at Addgene (https://www.addgene.org/Yulong_Li/). These include PGE2-1.0 (Addgene: 251353 for pDisplay backbone; 251355 for pAAV backbone) and PGE2-mut (Addgene: 251354 for pDisplay backbone; 251356 for pAAV backbone).

Data and code availability

Data and custom programs are available from the lead contact upon request.

ACKNOWLEDGMENTS

This research was supported by grants from the National Major Project of China Science and Technology Innovation 2030 for Brain Science and Brain-Inspired Technology (2022ZD0205600), the Postdoctoral Science Foundation (2022M720258), and the Boehringer Ingelheim-Peking University Postdoctoral Program to J.W.; the National Natural Science Foundation of China (31925017), the National Key R&D Program of China (2022YFE0108700 and 2023YFE0207100), the Beijing Municipal Science & Technology Commission (Z220009), the Feng Foundation of Biomedical Research, the Clement and Xinxin Foundation, and the New Cornerstone Science Foundation through the New Cornerstone Investigator Program to Y.L.; and the Peking-Tsinghua Center for Life Sciences and the State Key Laboratory of Membrane Biology at Peking University School of Life Sciences to Y.L.

We thank Xiaoguang Lei at Peking University Center for Life Sciences (PKU-CLS) and the optical imaging platform and small animal imaging platform of the National Center for Protein Sciences at Peking University in Beijing, China, for their support and assistance with the Opera Phenix, the Operetta CLS high-content imaging system, the Nikon A1RSi+ laser scanning microscope, and the behavior facility. We thank the Laboratory Animal Center of Peking University for advice and technical support. Cartoon illustrations, including Figures 2I, 2L1, 2M1, 3A, 3D, 3G, 4A, and S4A, were created with BioRender.com.

AUTHOR CONTRIBUTIONS

Y.L. supervised the study. L.W. and Y. Yang performed experiments related to sensor development, optimization, characterization in HEK293T cells and cultured neurons, sensor validation on acute brain slices, *in vivo* fiber photometry, and wide-field imaging experiments in living mice. Y. Yan performed characterization of the sensor's downstream coupling. F.D. initiated and helped with experiments related to *in vivo* wide-field imaging. H.W., B.L., and J.W. performed experiments related to characterization of the sensor in HEK293T cells. All authors contributed to the interpretation and analysis of the data. L.W. and Y.L. wrote the manuscript with contributions from all authors.

DECLARATION OF INTERESTS

Y.L. is a member of *Neuron*'s advisory board.

STAR★METHODS

Detailed methods are provided in the online version of this paper and include the following:

- KEY RESOURCES TABLE
- EXPERIMENTAL MODEL AND STUDY PARTICPANT DETAILS
  - Cell lines
  - Neuronal cultures and viral infection
  - Animals
- METHOD DETAILS
  - Molecular cloning
  - High-content imaging platform
  - Measurements of spectra
  - Measurements of kinetics
  - Luciferase complementation assay
  - Tango assay
  - Confocal microscopy
  - Preparation and imaging of acute brain slices
  - AAV injection and optic fiber implantation
  - Fiber photometry recording
  - Mice body temperature recording
  - Wide-field imaging
- QUANTIFICATION AND STATISTICAL ANALYSIS

SUPPLEMENTAL INFORMATION

Supplemental information can be found online at https://doi.org/10.1016/j.neuron.2026.01.030.

Received: April 17, 2025
Revised: December 14, 2025
Accepted: January 26, 2026

REFERENCES

1. Smith, W.L. (1989). The eicosanoids and their biochemical mechanisms of action. Biochem. J. *259*, 315–324. https://doi.org/10.1042/bj2590315.
2. Serhan, C.N., and Levy, B. (2003). Success of prostaglandin E2 in structure–function is a challenge for structure-based therapeutics. Proc. Natl. Acad. Sci. USA *100*, 8609–8611. https://doi.org/10.1073/pnas.1733589100.
3. Ricciotti, E., and FitzGerald, G.A. (2011). Prostaglandins and Inflammation. Arterioscler. Thromb. Vasc. Biol. *31*, 986–1000. https://doi.org/10.1161/ATVBAHA.110.207449.
4. Vane, J.R. (1971). Inhibition of Prostaglandin Synthesis as a Mechanism of Action for Aspirin-like Drugs. Nat. New Biol. *231*, 232–235. https://doi.org/10.1038/newbio231232a0.
5. Mahdi, J.G. (2010). Medicinal potential of willow: A chemical perspective of aspirin discovery. J. Saudi Chem. Soc. *14*, 317–322. https://doi.org/10.1016/j.jscs.2010.04.010.
6. Park, J.Y., Pillinger, M.H., and Abramson, S.B. (2006). Prostaglandin E2 synthesis and secretion: The role of PGE2 synthases. Clin. Immunol. *119*, 229–240. https://doi.org/10.1016/j.clim.2006.01.016.
7. Smith, W.L., DeWitt, D.L., and Garavito, R.M. (2000). Cyclooxygenases: Structural, Cellular, and Molecular Biology. Annu. Rev. Biochem. *69*, 145–182. https://doi.org/10.1146/annurev.biochem.69.1.145.
8. Candelario-Jalil, E., Slawik, H., Ridelis, I., Waschbisch, A., Akundi, R.S., Hüll, M., and Fiebich, B.L. (2005). Regional distribution of the prostaglandin E2 receptor EP1 in the rat brain: Accumulation in Purkinje cells of the cerebellum. J. Mol. Neurosci. *27*, 303–310. https://doi.org/10.1385/JMN:27:3:303.
9. Vasilache, A.M., Andersson, J., and Nilsberth, C. (2007). Expression of PGE2 EP3 receptor subtypes in the mouse preoptic region. Neurosci. Lett. *423*, 179–183. https://doi.org/10.1016/j.neulet.2007.06.048.
10. Andreasson, K. (2010). Emerging roles of PGE2 receptors in models of neurological disease. Prostaglandins Other Lipid Mediat. *91*, 104–112. https://doi.org/10.1016/j.prostaglandins.2009.04.003.
11. Abramovitz, M., Adam, M., Boie, Y., Carrière, M.-C., Denis, D., Godbout, C., Lamontagne, S., Rochette, C., Sawyer, N., Tremblay, N.M., et al. (2000). The utilization of recombinant prostanoid receptors to determine the affinities and selectivities of prostaglandins and related analogs. Biochim. Biophys. Acta *1483*, 285–293. https://doi.org/10.1016/S1388-1981(99)00164-X.
12. Funk, C.D. (2001). Prostaglandins and Leukotrienes: Advances in Eicosanoid Biology. Science *294*, 1871–1875. https://doi.org/10.1126/science.294.5548.1871.
13. Thorén, S., and Jakobsson, P.J. (2000). Coordinate up- and down-regulation of glutathione-dependent prostaglandin E synthase and cyclooxygenase-2 in A549 cells. Inhibition by NS-398 and leukotriene C4. Eur. J. Biochem. *267*, 6428–6434. https://doi.org/10.1046/j.1432-1327.2000.01735.x.
14. Murakami, M., Naraba, H., Tanioka, T., Semmyo, N., Nakatani, Y., Kojima, F., Ikeda, T., Fueki, M., Ueno, A., Oh-ishi, S., et al. (2000). Regulation of Prostaglandin E2 Biosynthesis by Inducible Membrane-associated Prostaglandin E2 Synthase That Acts in Concert with Cyclooxygenase-2. J. Biol. Chem. *275*, 32783–32792. https://doi.org/10.1074/jbc.M003505200.
15. Jaffe, B.M., Smith, J.W., Newton, W.T., and Parker, C.W. (1971). Radioimmunoassay for Prostaglandins. Science *171*, 494–496. https://doi.org/10.1126/science.171.3970.494.
16. Ciceri, P., Zhang, Y., Shaffer, A.F., Leahy, K.M., Woerner, M.B., Smith, W.G., Seibert, K., and Isakson, P.C. (2002). Pharmacology of Celecoxib in Rat Brain after Kainate Administration. J. Pharmacol. Exp. Ther. *302*, 846–852. https://doi.org/10.1124/jpet.302.3.846.
17. Aroonrerk, N., Suksamrarn, A., and Kirtikara, K. (2007). A Sensitive Direct ELISA for Detection of Prostaglandin E2. J. Immunoassay Immunochem. *28*, 319–330. https://doi.org/10.1080/15321810701603450.
18. Zhou, C., Satpute, V., Yip, K.L., Anderson, L.L., Hawkins, N., Kearney, J., and Arnold, J.C. (2024). A high seizure burden increases several prostaglandin species in the hippocampus of a *Scn1a*$^{+/-}$ mouse model of Dravet syndrome. Prostaglandins Other Lipid Mediat. *172*, 106836. https://doi.org/10.1016/j.prostaglandins.2024.106836.
19. Golovko, M.Y., and Murphy, E.J. (2008). An improved LC-MS/MS procedure for brain prostanoid analysis using brain fixation with head-focused microwave irradiation and liquid-liquid extraction. J. Lipid Res. *49*, 893–902. https://doi.org/10.1194/jlr.D700030-JLR200.
20. Sehic, E., Székely, M., Ungar, A.L., Oladehin, A., and Blatteis, C.M. (1996). Hypothalamic prostaglandin E2 during lipopolysaccharide-induced fever in guinea pigs. Brain Res. Bull. *39*, 391–399. https://doi.org/10.1016/0361-9230(96)00037-8.
21. Chefer, V.I., Thompson, A.C., Zapata, A., and Shippenberg, T.S. (2009). Overview of brain microdialysis. Curr. Protoc. Neurosci. *Chapter 7*, Unit7.1. https://doi.org/10.1002/0471142301.ns0701s47.
22. Sun, F., Zeng, J., Jing, M., Zhou, J., Feng, J., Owen, S.F., Luo, Y., Li, F., Wang, H., Yamaguchi, T., et al. (2018). A Genetically Encoded Fluorescent Sensor Enables Rapid and Specific Detection of Dopamine in Flies, Fish, and Mice. Cell *174*, 481–496.e19. https://doi.org/10.1016/j.cell.2018.06.042.
23. Jing, M., Zhang, P., Wang, G., Feng, J., Mesik, L., Zeng, J., Jiang, H., Wang, S., Looby, J.C., Guagliardo, N.A., et al. (2018). A genetically encoded fluorescent acetylcholine indicator for in vitro and in vivo studies. Nat. Biotechnol. *36*, 726–737. https://doi.org/10.1038/nbt.4184.
24. Feng, J., Zhang, C., Lischinsky, J.E., Jing, M., Zhou, J., Wang, H., Zhang, Y., Dong, A., Wu, Z., Wu, H., et al. (2019). A Genetically Encoded Fluorescent Sensor for Rapid and Specific In Vivo Detection of Norepinephrine. Neuron *102*, 745–761.e8. https://doi.org/10.1016/j.neuron.2019.02.037.
25. Wang, H., Qian, T., Zhao, Y., Zhuo, Y., Wu, C., Osakada, T., Chen, P., Chen, Z., Ren, H., Yan, Y., et al. (2023). A tool kit of highly selective and sensitive genetically encoded neuropeptide sensors. Science *382*, eabq8173. https://doi.org/10.1126/science.abq8173.
26. Jing, M., Li, Y., Zeng, J., Huang, P., Skirzewski, M., Kljakic, O., Peng, W., Qian, T., Tan, K., Zou, J., et al. (2020). An optimized acetylcholine sensor for monitoring in vivo cholinergic activity. Nat. Methods *17*, 1139–1146. https://doi.org/10.1038/s41592-020-0953-2.
27. Sun, F., Zhou, J., Dai, B., Qian, T., Zeng, J., Li, X., Zhuo, Y., Zhang, Y., Wang, Y., Qian, C., et al. (2020). Next-generation GRAB sensors for monitoring dopaminergic activity in vivo. Nat. Methods *17*, 1156–1166. https://doi.org/10.1038/s41592-020-00981-9.
28. Dong, A., He, K., Dudok, B., Farrell, J.S., Guan, W., Liput, D.J., Puhl, H.L., Cai, R., Wang, H., Duan, J., et al. (2022). A fluorescent sensor for spatiotemporally resolved imaging of endocannabinoid dynamics in vivo. Nat. Biotechnol. *40*, 787–798. https://doi.org/10.1038/s41587-021-01074-4.
29. Qu, C., Mao, C., Xiao, P., Shen, Q., Zhong, Y.-N., Yang, F., Shen, D.-D., Tao, X., Zhang, H., Yan, X., et al. (2021). Ligand recognition, unconventional activation, and G protein coupling of the prostaglandin E2 receptor EP2 subtype. Sci. Adv. *7*, eabf1268. https://doi.org/10.1126/sciadv.abf1268.
30. Di Rosa, M., Giroud, J.P., and Willoughby, D.A. (1971). Studies of the mediators of the acute inflammatory response induced in rats in different sites

by carrageenan and turpentine. J. Pathol. *104*, 15–29. https://doi.org/10.1002/path.1711040103.

31. Yamagata, K., Andreasson, K.I., Kaufmann, W.E., Barnes, C.A., and Worley, P.F. (1993). Expression of a mitogen-inducible cyclooxygenase in brain neurons: Regulation by synaptic activity and glucocorticoids. Neuron *11*, 371–386. https://doi.org/10.1016/0896-6273(93)90192-T.
32. Romanovsky, A.A., Kulchitsky, V.A., Akulich, N.V., Koulchitsky, S.V., Simons, C.T., Sessler, D.I., and Gourine, V.N. (1996). First and second phases of biphasic fever: two sequential stages of the sickness syndrome? Am. J. Physiol. *271*, R244–R253. https://doi.org/10.1152/ajpregu.1996.271.1.R244.
33. Ushikubi, F., Segi, E., Sugimoto, Y., Murata, T., Matsuoka, T., Kobayashi, T., Hizaki, H., Tuboi, K., Katsuyama, M., Ichikawa, A., et al. (1998). Impaired febrile response in mice lacking the prostaglandin E receptor subtype EP3. Nature *395*, 281–284. https://doi.org/10.1038/26233.
34. Oka, T., Oka, K., Kobayashi, T., Sugimoto, Y., Ichikawa, A., Ushikubi, F., Narumiya, S., and Saper, C.B. (2003). Characteristics of thermoregulatory and febrile responses in mice deficient in prostaglandin EP1 and EP3 receptors. J. Physiol. *551*, 945–954. https://doi.org/10.1113/jphysiol.2003.048140.
35. Lazarus, M., Yoshida, K., Coppari, R., Bass, C.E., Mochizuki, T., Lowell, B.B., and Saper, C.B. (2007). EP3 prostaglandin receptors in the median preoptic nucleus are critical for fever responses. Nat. Neurosci. *10*, 1131–1133. https://doi.org/10.1038/nn1949.
36. Ek, M., Arias, C., Sawchenko, P., and Ericsson-Dahlstrand, A. (2000). Distribution of the EP3 prostaglandin E2 receptor subtype in the rat brain: Relationship to sites of interleukin-1-induced cellular responsiveness. J. Comp. Neurol. *428*, 5–20. https://doi.org/10.1002/1096-9861(20001204)428:1<5::AID-CNE2>3.0.CO;2-M.
37. Li, S., Wang, Y., Matsumura, K., Ballou, L.R., Morham, S.G., and Blatteis, C.M. (1999). The febrile response to lipopolysaccharide is blocked in cyclooxygenase-$2^{-/-}$, but not in cyclooxygenase-$1^{-/-}$ mice. Brain Res. *825*, 86–94. https://doi.org/10.1016/S0006-8993(99)01225-1.
38. Shionoya, K., Eskilsson, A., and Blomqvist, A. (2022). Prostaglandin production selectively in brain endothelial cells is both necessary and sufficient for eliciting fever. Proc. Natl. Acad. Sci. USA *119*, e2122562119. https://doi.org/10.1073/pnas.2122562119.
39. Navarro, E., Romero, S.D., and Yaksh, T.L. (1989). CNS Stimulation and PGE2 Release. III. Pentamethylenetetrazole-Induced Seizures. J. Cereb. Blood Flow Metab. *9*, 180–186. https://doi.org/10.1038/jcbfm.1989.27.
40. Vezzani, A., and Granata, T. (2005). Brain Inflammation in Epilepsy: Experimental and Clinical Evidence. Epilepsia *46*, 1724–1743. https://doi.org/10.1111/j.1528-1167.2005.00298.x.
41. Riazi, K., Galic, M.A., and Pittman, Q.J. (2010). Contributions of peripheral inflammation to seizure susceptibility: Cytokines and brain excitability. Epilepsy Res. *89*, 34–42. https://doi.org/10.1016/j.eplepsyres.2009.09.004.
42. Serrano, G.E., Lelutiu, N., Rojas, A., Cochi, S., Shaw, R., Makinson, C.D., Wang, D., FitzGerald, G.A., and Dingledine, R. (2011). Ablation of Cyclooxygenase-2 in Forebrain Neurons is Neuroprotective and Dampens Brain Inflammation after Status Epilepticus. J. Neurosci. *31*, 14850–14860. https://doi.org/10.1523/JNEUROSCI.3922-11.2011.
43. Dana, H., Mohar, B., Sun, Y., Narayan, S., Gordus, A., Hasseman, J.P., Tsegaye, G., Holt, G.T., Hu, A., Walpita, D., et al. (2016). Sensitive red protein calcium indicators for imaging neural activity. eLife *5*, e12727. https://doi.org/10.7554/eLife.12727.
44. Ayoub, S.S., Botting, R.M., Goorha, S., Colville-Nash, P.R., Willoughby, D.A., and Ballou, L.R. (2004). Acetaminophen-induced hypothermia in mice is mediated by a prostaglandin endoperoxide synthase 1 gene-derived protein. Proc. Natl. Acad. Sci. USA *101*, 11165–11169. https://doi.org/10.1073/pnas.0404185101.
45. Marcheselli, V.L., and Bazan, N.G. (1996). Sustained Induction of Prostaglandin Endoperoxide Synthase-2 by Seizures in Hippocampus: INHIBITION BY A PLATELET-ACTIVATING FACTOR ANTAGONIST. J. Biol. Chem. *271*, 24794–24799. https://doi.org/10.1074/jbc.271.40.24794.
46. Hinz, B., and Brune, K. (2002). Cyclooxygenase-2—10 Years Later. J. Pharmacol. Exp. Ther. *300*, 367–375. https://doi.org/10.1124/jpet.300.2.367.
47. Yoshikawa, K., Kita, Y., Kishimoto, K., and Shimizu, T. (2006). Profiling of Eicosanoid Production in the Rat Hippocampus during Kainic Acid-induced Seizure: DUAL PHASE REGULATION AND DIFFERENTIAL INVOLVEMENT OF COX-1 AND COX-2. J. Biol. Chem. *281*, 14663–14669. https://doi.org/10.1074/jbc.M511089200.
48. Jiang, J., Ganesh, T., Du, Y., Quan, Y., Serrano, G., Qui, M., Speigel, I., Rojas, A., Lelutiu, N., and Dingledine, R. (2012). Small molecule antagonist reveals seizure-induced mediation of neuronal injury by prostaglandin E2 receptor subtype EP2. Proc. Natl. Acad. Sci. USA *109*, 3149–3154. https://doi.org/10.1073/pnas.1120195109.
49. Jakobsson, P.J., Thorén, S., Morgenstern, R., and Samuelsson, B. (1999). Identification of human prostaglandin E synthase: A microsomal, glutathione-dependent, inducible enzyme, constituting a potential novel drug target. Proc. Natl. Acad. Sci. USA *96*, 7220–7225. https://doi.org/10.1073/pnas.96.13.7220.
50. Choi, S.-H., Aid, S., and Bosetti, F. (2009). The distinct roles of cyclooxygenase-1 and -2 in neuroinflammation: implications for translational research. Trends Pharmacol. Sci. *30*, 174–181. https://doi.org/10.1016/j.tips.2009.01.002.
51. Elander, L., Engström, L., Ruud, J., Mackerlova, L., Jakobsson, P.-J., Engblom, D., Nilsberth, C., and Blomqvist, A. (2009). Inducible Prostaglandin E2 Synthesis Interacts in a Temporally Supplementary Sequence with Constitutive Prostaglandin-Synthesizing Enzymes in Creating the Hypothalamic–Pituitary–Adrenal Axis Response to Immune Challenge. J. Neurosci. *29*, 1404–1413. https://doi.org/10.1523/JNEUROSCI.5247-08.2009.
52. Elander, L., Ruud, J., Korotkova, M., Jakobsson, P.-J., and Blomqvist, A. (2010). Cyclooxygenase-1 mediates the immediate corticosterone response to peripheral immune challenge induced by lipopolysaccharide. Neurosci. Lett. *470*, 10–12. https://doi.org/10.1016/j.neulet.2009.12.036.
53. Furuyashiki, T., and Narumiya, S. (2011). Stress responses: the contribution of prostaglandin E2 and its receptors. Nat. Rev. Endocrinol. *7*, 163–175. https://doi.org/10.1038/nrendo.2010.194.
54. Kaufmann, W.E., Worley, P.F., Pegg, J., Bremer, M., and Isakson, P. (1996). COX-2, a synaptically induced enzyme, is expressed by excitatory neurons at postsynaptic sites in rat cerebral cortex. Proc. Natl. Acad. Sci. USA *93*, 2317–2321. https://doi.org/10.1073/pnas.93.6.2317.
55. Kirkby, N.S., Zaiss, A.K., Urquhart, P., Jiao, J., Austin, P.J., Al-Yamani, M., Lundberg, M.H., MacKenzie, L.S., Warner, T.D., Nicolaou, A., et al. (2013). LC-MS/MS Confirms That COX-1 Drives Vascular Prostacyclin Whilst Gene Expression Pattern Reveals Non-Vascular Sites of COX-2 Expression. PLoS one *8*, e69524. https://doi.org/10.1371/journal.pone.0069524.
56. Moore, S.A., Spector, A.A., and Hart, M.N. (1988). Eicosanoid metabolism in cerebromicrovascular endothelium. Am. J. Physiol. *254*, C37–C44. https://doi.org/10.1152/ajpcell.1988.254.1.C37.
57. Cao, C., Matsumura, K., Yamagata, K., and Watanabe, Y. (1995). Induction by lipopolysaccharide of cyclooxygenase-2 mRNA in rat brain; its possible role in the febrile response. Brain Res. *697*, 187–196. https://doi.org/10.1016/0006-8993(95)00839-I.
58. Elmquist, J.K., Scammell, T.E., and Saper, C.B. (1997). Mechanisms of CNS response to systemic immune challenge: the febrile response. Trends Neurosci. *20*, 565–570. https://doi.org/10.1016/S0166-2236(97)01138-7.
59. Wilhelms, D.B., Kirilov, M., Mirrasekhian, E., Eskilsson, A., Kugelberg, U.Ö., Klar, C., Ridder, D.A., Herschman, H.R., Schwaninger, M., Blomqvist, A., et al. (2014). Deletion of Prostaglandin E2 Synthesizing Enzymes in Brain Endothelial Cells Attenuates Inflammatory Fever.

J. Neurosci. *34*, 11684–11690. https://doi.org/10.1523/JNEUROSCI.1838-14.2014.

60. Yamagata, K., Matsumura, K., Inoue, W., Shiraki, T., Suzuki, K., Yasuda, S., Sugiura, H., Cao, C., Watanabe, Y., and Kobayashi, S. (2001). Coexpression of Microsomal-Type Prostaglandin E Synthase with Cyclooxygenase-2 in Brain Endothelial Cells of Rats during Endotoxin-Induced Fever. J. Neurosci. *21*, 2669–2677. https://doi.org/10.1523/JNEUROSCI.21-08-02669.2001.

61. Engström, L., Ruud, J., Eskilsson, A., Larsson, A., Mackerlova, L., Kugelberg, U., Qian, H., Vasilache, A.M., Larsson, P., Engblom, D., et al. (2012). Lipopolysaccharide-Induced Fever Depends on Prostaglandin E2 Production Specifically in Brain Endothelial Cells. Endocrinology *153*, 4849–4861. https://doi.org/10.1210/en.2012-1375.

62. Nilsson, A., Wilhelms, D.B., Mirrasekhian, E., Jaarola, M., Blomqvist, A., and Engblom, D. (2017). Inflammation-induced anorexia and fever are elicited by distinct prostaglandin dependent mechanisms, whereas conditioned taste aversion is prostaglandin independent. Brain Behav. Immun. *61*, 236–243. https://doi.org/10.1016/j.bbi.2016.12.007.

63. Deng, F., Wan, J., Li, G., Dong, H., Xia, X., Wang, Y., Li, X., Zhuang, C., Zheng, Y., Liu, L., et al. (2024). Improved green and red GRAB sensors for monitoring spatiotemporal serotonin release in vivo. Nat. Methods *21*, 692–702. https://doi.org/10.1038/s41592-024-02188-8.

64. Wan, Q., Okashah, N., Inoue, A., Nehmé, R., Carpenter, B., Tate, C.G., and Lambert, N.A. (2018). Mini G protein probes for active G protein–coupled receptors (GPCRs) in live cells. J. Biol. Chem. *293*, 7466–7473. https://doi.org/10.1074/jbc.RA118.001975.

65. Racine, R.J. (1972). Modification of seizure activity by electrical stimulation: II. Motor seizure. Electroencephalogr. Clin. Neurophysiol. *32*, 281–294. https://doi.org/10.1016/0013-4694(72)90177-0.

STAR★METHODS

KEY RESOURCES TABLE

REAGENT or RESOURCE	SOURCE	IDENTIFIER
Bacterial and virus strains		
AAV2/9-EF1α-PGE2-1.0 ($GRAB_{PGE2-1.0}$)	This paper; WZ Biosciences	YL025001-AV9
AAV2/9-EF1α-PGE2mut ($GRAB_{PGE2mut}$)	This paper; WZ Biosciences	YL024005-AV9
AAV9-hSyn-NES-jRGECO1a-WPRE	WZ Biosciences	AV203018-AV9
Chemicals, peptides, and recombinant proteins		
Prostaglandin E2	Santa cruz	Cat#sc-201225A
PF-04418948	MedChemExpress	Cat#1078166-57-0
IL-1β (protein, mouse)	Novoprotein	Cat#C042
Pentylenetetrazole (PTZ)	aladdin	Cat#P103065
Lipopolysaccharides (LPSs)	Sigma-Aldrich	Cat#L5886
Indomethacin	MedChemExpress	Cat#53-86-1
Kainic acid	Cayman	Cat#78050
Prostaglandin D2	Cayman	Cat#41598-07-6
Prostaglandin F2α	Santa cruz	Cat#38562-01-5
Prostaglandin I2 sodium	Santa cruz	Cat#sc-201231
Docosahexaenoic Acid (DHA)	Cayman	Cat#90310
Sphingosine-1-phosphate (S1P)	Cayman	Cat#62570
1-Oleoyl Lysophosphatidic Acid (1-Oleoyl LPA)	Cayman	Cat#10010093
AEA	Cayman	Cat#90050
2-AG	Tocris	Cat#1298
PAF	Apexbio	Cat#B7227
L-Glutamic acid (Glu)	Sigma-Aldrich	Cat#V900408
γ-Aminobutyric acid (GABA)	Tocris	Cat#0344
Acetylcholine chloride (ACh)	Solarbio	Cat#G8320
Serotonin hydrochloride (5-HT)	Tocris	Cat#3547
Norepinephrinebitartrate (NE)	Tocris	Cat#5169
Dopamine hydrochloride (DA)	Sigma-Aldrich	Cat#H8502
Histamine dihydrochloride (HA)	Tocris	Cat#3545
2,2,2-Tribromoethanol (Avetin)	Sigma-Aldrich	Cat#T48402
Isoflurane	RWD Life Science	Cat#R510-22
Experimental models: Cell lines		
HEK293T	ATCC	Cat#CRL-3216;RRID:CVCL_0063
HTLA cells for Tango assay	Gift from Bryan L. Roth	N/A
Experimental models: Organisms/strains		
Rat: wild-type Sprague-Dawley rat pups (P0)	Beijing Vital River Laboratory Animal Technology Co., Ltd.	N/A
Mouse: wild-type C57BL/6	Beijing Vital River Laboratory Animal Technology Co., Ltd.	N/A
Recombinant DNA		
Plasmid: pDisplay vector	Invitrogen	Cat#V66020
Plasmid: pDisplay-PGE2-1.0-IRES-mCherry-CAAX	This paper	N/A
Plasmid: pDisplay-PGE2mut-IRES-mCherry-CAAX	This paper	N/A
Plasmid: pAAV-EF1α-PGE2-1.0	This paper	N/A
Plasmid: pAAV-EF1α-PGE2mut	This paper	N/A

(*Continued on next page*)

Please cite this article in press as: Wang et al., A genetically encoded fluorescent sensor for monitoring spatiotemporal prostaglandin E2 dynamics *in vivo*, Neuron (2026), https://doi.org/10.1016/j.neuron.2026.01.030

Continued

REAGENT or RESOURCE	SOURCE	IDENTIFIER
Plasmid: PGE2-1.0-SmBit	This paper	N/A
Plasmid: EP2-SmBit	This paper	N/A
Software and algorithms		
Arduino	Arduino.cc	https://www.arduino.cc; RRID: SCR_017284
ImageJ	NIH	https://imagej.nih.gov/ij/; RRID: SCR_003070
Matlab R2020a	MathWorks	https://www.mathworks.com/; RRID:SCR_001622
Origin Pro	OriginLab	https://www.originlab.com/; RRID: SCR_014212
Spike2	Cambridge Electronic Design Ltd.	https://ced.co.uk/products/spkovin; RRID: SCR_000903

EXPERIMENTAL MODEL AND STUDY PARTICPANT DETAILS

Cell lines

HEK293T cells were cultured in DPF medium (high-glucose DMEM supplemented with 10% fetal bovine serum, 100 U/mL penicillin, and 0.1 mg/mL streptomycin) at 37°C in humidified air containing 5% CO_2. Cells at 60–70% confluence were transfected with a 3:1 mass ratio of polyethyleneimine (PEI) to plasmid DNA. In brief, PEI and plasmid DNA were combined in a microtube, and after 15 min at room temperature the PEI-DNA mixture was added to the cells; the medium was changed approximately 6 h later. The cells were then allowed to express the plasmid DNA for 24–48 h before imaging.

Neuronal cultures and viral infection

Primary neurons were derived from P0 Sprague-Dawley rat pups. The cerebral cortex was dissected and cortical neurons were dissociated by using 0.25% trypsin-EDTA. Then, neurons were plated on 12 mm diameter glass coverslips (previously sterilized and coated with poly-D-lysine) and cultured in Neurobasal medium supplemented with 2% B-27, 1% GlutaMAX, 100 U/mL penicillin, and 0.1 mg/mL streptomycin; every 3 days, half of the medium was replaced with fresh medium. Adeno-associated virus (AAV, 1 μL, at a titer of about 3×10^{12} vg/mL) was added to the neurons at 3–7 days *in vitro* (DIV3–7), and imaging was performed on DIV13–25.

Animals

All animal protocols were approved by the respective laboratory animal care and use committees at Peking University. The mice used were both male and female C57BL/6J mice (Charles River Laboratories). For these experiments, P0 and adult (age 6–12 months) mice were used; these mice were housed in a temperature-controlled animal facility with a 12-h light/dark cycle, with food and water available ad libitum. P0 Sprague-Dawley rats (Charles River Laboratories) of both sexes were used to prepare primary neuronal cultures as described above.

METHOD DETAILS

Molecular cloning

In this study, the molecular clones were generated using Gibson assembly. The DNA fragments were amplified with primers containing ~25 bp overlap. Sanger sequencing was used to confirm the sequence of all clones. All cDNAs encoding the candidate $GRAB_{PGE2}$ sensors were cloned into the pDisplay vector (Invitrogen) with an upstream IgK leader sequence and a downstream IRES-mCherry-CAAX cassette (to label the cell membrane and calibrate the sensor's fluorescence intensity). To measure downstream signaling using the Tango assay, genes encoding wild-type EP2 and the PGE2-1.0 sensor were cloned into the pTango vector. To express the sensors in cultured neurons, acute brain slices, and living mice, sequences encoding PGE2-1.0 and PGE2mut were cloned into the pAAV vector.

High-content imaging platform

HEK293T cells cultured in CellCarrier Ultra-Black 96-well plates were imaged using an Opera Phenix high-content imaging analysis system (PerkinElmer) equipped with 20× air, 40× air, and 40× water-immersion objectives, using 488 nm and 561 nm lasers for excitation. The signals from the green and red fluorescent proteins were collected via 525/50-nm and 600/30-nm filters, respectively. The accompanying software package Harmony (PerkinElmer) was used to analyze the fluorescence signals, localizing the cell membranes in the field of view using the membrane-targeted mCherry red fluorescence signal and delineating regions of interest (ROIs). The ratio between green and red fluorescence intensity was calculated and used to measure the brightness of the green sensor (i.e., the corrected F value). The change in the sensor's fluorescence intensity was calculated using the formula $\Delta F/F_0$, where F_0 is baseline fluorescence.

Measurements of spectra

For one-photon spectra, HEK293T cells expressing PGE2-1.0 were collected and transferred to a 384-well plate in the absence or presence of 10 μM PGE2. Excitation and emission spectra were measured at 5 nm increments with a 20 nm bandwidth using a Safire2 multi-mode plate reader (Tecan). Control cells not expressing a sensor were prepared to the same density and were measured using the same protocol for background subtraction. For two-photon spectra, HEK293T cells expressing PGE2-1.0 were cultured on 12 mm coverslips. The two-photon excitation spectrum was measured at 10 nm increments and ranging from 700 to 1050 nm using an Ultima Investigator two-photon microscope (Bruker) equipped with a ×20/1.0 NA water-immersion objective (Olympus), an InSight X3 tunable laser (Spectra-Physics) and the Prairie View 5.5 software (Bruker).

Measurements of kinetics

The kinetics of the PGE2-1.0 sensor were measured as previously reported.[63] The local puff system utilized is a valve-based, pressure-driven picospritzer (PV800 Pneumatic PicoPump, WPI). A glass pipette tip, controlled by the picospritzer and filled with either 10 μM PGE2 or EP2 antagonist (PF04418948) was positioned within ~10 μm of the PGE2-1.0 sensor-expressing HEK293T cells for focal delivery. The line-scanning mode (256 fps) of the confocal microscope was used to record rapid changes in fluorescence. The PGE2 or EP2 antagonist (PF04418948) was puffed from the pipette to measure the on and off response kinetics, respectively.

Luciferase complementation assay

The HEK293T cells were transfected with the wild-type EP2 receptor, the PGE2-1.0 sensor, or Gs-LgBit alone. The luciferase complementation assay was performed as previously described.[64] In brief, 24–36 h after transfection, the cells were dissociated using a cell scraper, resuspended in PBS, and transferred to 96-well plates. Then, 5 μM furimazine (NanoLuc Luciferase Assay, Promega) and PGE2 at various concentrations (ranging from 0.01 nM to 10 μM) were bath-applied to the cells. After incubation for 10 min in the dark, luminescence was measured using a VICTOR X5 multilabel plate reader (PerkinElmer).

Tango assay

A reporter cell line, HTLA cells that stably express a tTA-dependent luciferase reporter and a β-arrestin2-TEV fusion gene, was transfected with pTango vectors to express wild-type EP2 receptor or the PGE2-1.0 sensor, and the empty vector was used as a control. At 24 h after transfection, the cells were transferred to 96-well plates and bathed with PGE2 at varying concentrations (ranging from 0.01 nM to 30 μM). The cells were then cultured for 12 h to allow the expression of tTA-dependent luciferase. Bright-Glo reagent (Fluc Luciferase Assay System, Promega) was added to a final concentration of 5 μM, and luminescence was measured using a VICTOR X5 multilabel plate reader (PerkinElmer).

Confocal microscopy

Confocal microscopy was performed using a Nikon Ti-E A1 laser-scanning confocal microscope equipped with a 10×/0.45-NA objective, a 20×/0.75-NA objective, and a 40×/1.35-NA oil-immersion objective; a 488 nm laser was used for excitation, and fluorescence was collected via a 525/50-nm filter. During imaging, the coverslip was placed in a custom-made imaging chamber at room temperature (24°C). The microscope was controlled using NIS-Elements (Nikon), and the data were processed and analyzed using ImageJ software.

Preparation and imaging of acute brain slices

Adult mice were anesthetized by an i.p. injection of avertin (240 mg/kg; Sigma-Aldrich) and then placed in a stereotaxic frame for injection of AAVs. A microinjection pump (Nanoliter 2000 Injector, WPI) was used for injecting 300 nL of virus (AAV2/9-EF1α-PGE2-1.0, 2.68×1012 vg/mL; or AAV2/9-EF1α-PGE2mut, 1×1013 vg/mL, both packaged by BrainVTA) at the CA1 region using the following coordinates: AP, -2 mm relative to Bregma; ML, -1.3 mm relative to Bregma; and DV, -1.5 mm. Two weeks after viral injection, mice were again anesthetized and transcardial perfusion was performed using cold oxygenated slicing buffer containing (in mM) 110 choline chloride, 2.5 KCl, 1 NaH_2PO_4, 25 $NaHCO_3$, 7 $MgCl_2$, 25 glucose, 0.5 $CaCl_2$, 1.3 sodium ascorbate and 0.6 sodium pyruvate. Brains were then rapidly removed and sectioned into 300-μm-thick coronal slices with a VT1200 vibratome (Leica). The acute brain slices were incubated at 34°C for at least 40 min in oxygen-saturated Ringer's buffer containing (in mM) 125 NaCl, 2.5 KCl, 1 NaH_2PO_4, 25 $NaHCO_3$, 1.3 $MgCl_2$, 25 glucose, 2 $CaCl_2$, 1.3 sodium ascorbate and 0.6 sodium pyruvate, and then transferred to a custom-made recording chamber. The Prairie View 5.5.64.100 software with an Ultima Investigator two-photon microscope (Bruker) equipped with a ×16/0.80-NA water-immersion objective (Olympus) and an InSight X3 tunable laser (Spectra-Physics) were used for data collection. A 920-nm laser was used for excitation, and a 525/70-nm emission filter was used to collect the fluorescence signal. During imaging, the acute brain slices were continuously perfused with artificial cerebrospinal fluid (ACSF). The perfusion was controlled by a peristaltic pump (NKCP-S10B, Kamoer) delivering solution at a constant flow rate. For drug application, the perfusion solution was switched from standard ACSF to ACSF containing different drugs (10ng/mL IL-1β / 15 mM PTZ / 10 μM PGE2 /10 μM PGD2 /10 μM PGF2α). The start time of drug application was defined as the moment the drug-containing solution reached the imaging chamber.

AAV injection and optic fiber implantation

To anesthetize adult mice, 2,2,2-tribromoethanol (Avertin, 240 mg/kg body weight, Sigma-Aldrich) was administered by i.p. injection. The anesthetized mice were then secured in a stereotaxic frame for AAV injection. Using a microinjection pump (Nanoliter 2000 Injector, WPI), 300 nL of virus (AAV2/9-EF1α-PGE2-1.0, 2.68×10^{12} vg/mL, packaged by BrainVTA) was slowly injected into the median preoptic nucleus (MnPO) of the hypothalamus using the following coordinates: AP, 0 mm relative to Bregma; ML, -0.6 mm relative to Bregma; and DV, -5 mm. After AAV injection, the needle was left in place for 5 min, and an optic fiber was implanted at the injection site. The entire setup was secured with dental cement, and recordings were performed after 14 days to allow for viral expression.

Fiber photometry recording

To collect the signal from the PGE2-1.0 sensor, we used an FPS-410/470/561 photometry system (Inper) with the Inper signal v.2.0.0 software (Inper). In brief, a 10-Hz (with 20-ms pulse duration) 470/5-nm filtered light-emitting diode (LED) at 20 μW was used to excite the green fluorescence and the emission light was collected at 520 nm. For recording, the mouse was connected to the fiber optic system and allowed to freely move around and acclimate in a behavioral chamber for approximately 30 min, during which the recorded fiber optic signals served as the baseline.

In the experiment inducing endogenous PGE2 release with lipopolysaccharide (LPS), a stock solution of LPS (5 mg/mL; Sigma, L4130) was diluted with saline and injected i.p. at 1 mg/kg body weight. For the cyclooxygenase inhibitor indomethacin (Indo, MedChemExpress, 53-86-1) the stock solution (10 mM) was diluted with 0.2 M Tris-HCl (pH 8) and injected i.p. at 15 mg/kg body weight. For IL-1β (Novoprotein, C042) the stock solution (100 μg/mL) was diluted with saline and injected i.p. at 25 μg/kg body weight.

Mice body temperature recording

During experiments, the mice were placed in the behavioral chamber situated in a temperature-controlled room, with an infrared thermal camera (Inf iRay, AT20) fixed at the top of the behavioral chamber to monitor mouse skin temperature through infrared imaging. The field of view of this camera covers the entire behavioral chamber so the free-moving mice could be monitored at any position. This camera could continuously monitor the temperature within its field of view and generate temperature readings at one-minute intervals. Each reading included the maximum, minimum, and average temperatures observed within the field of view. The maximum temperature recorded at each time point was utilized as an indication of the mice's skin temperature.

Wide-field imaging

Newborn (P0–P1) C57BL/6J pups received an injection of a 1:1 virus mixture containing AAV2/9-EF1α-PGE2-1.0 (2.68×10^{12} vg/mL, packaged by BrainVTA) and AAV2/9-hSyn-NES-jRGECO1a (8.3×10^{13} vg/mL, packaged by WZ Biosciences Inc.) in the transverse sinus on both hemispheres (3 μL per hemisphere) via a microinjection pump (KD Scientific, LEGATO 130). Prior to virus injection, the pups were anesthetized by placing them on ice for 1–2 min. When the pups stopped moving, they were then placed on a cold metal plate with ice packs to keep them cool, and their heads were secured. The skin on both sides of the transverse sinus was incised, and a glass electrode was used to puncture the wall of the transverse sinus, ensuring that the electrode tip was located inside the sinus. The virus mixture was then injected at a rate of 1.2 μL/min, after which the skin at the injection site was closed using tissue adhesive (3M Vetbond, 1469SB). The pups were then placed on a warming pad and monitored until they recovered; when they resumed normal activity, they were returned to their home cage.

The craniotomy procedure and implantation of EEG and EMG electrodes were performed 8–10 weeks after virus injection. The mice were anesthetized with Avertin (240 mg/kg body weight) and secured in a stereotaxic injector while maintaining inhalation anesthesia with 1% isoflurane. Erythromycin ointment was applied to the eyes, and the fur and scalp were removed from the top of the head, followed by cleaning the underlying connective tissue. A cranial drill was used to create an 8 mm × 8 mm window in the skull, and care was taken to remove the skull section. A custom-made thin glass coverslip of the same shape as the cranial window was affixed in place to replace the skull section and serve as an imaging window. Four EEG electrodes were also implanted: two near the frontal cortex in each hemisphere, one near the right hippocampal cortex, and one near the cerebellum. Finally, two EMG electrodes were inserted into the neck muscle tissue. The electrode micro-connectors were glued to the skull using cyanoacrylate adhesive, and a custom metal headpiece was attached to the mouse's head for subsequent head stabilization. The entire setup was secured with dental cement, while ensuring that the craniotomy window was not obscured. The mice were allowed to recover for 1–2 weeks, after which wide-field imaging experiments were performed.

A custom-built two-color wide-field microscope equipped with a 2×/0.5-NA objective (Olympus, MVPLAPO2XC) and two 1×/0.25-NA tube lenses (Olympus, MVPPLAPO1X) was used to expand the field of view. The signal was acquired using two high-speed, high-sensitivity sCMOS cameras (Andor, Zyla 4.2 PLUS). The excitation light was delivered via a fiber-coupled laser (Changchun New Industries Optoelectronics Technology Co., Ltd.) capable of emitting excitation light at 405 nm, 488 nm, and 561 nm. The emission light was passed through a 567 nm long-pass dichroic beam splitter (Thorlabs, DMLP567L) for spectral separation, and then through either a 525/36 nm or 609/34 nm emission filter (Chroma) before entering the green and red channels, respectively, of the sCMOS cameras. Images were acquired using Micro-Manager 2.0 software with a resolution of 512×512 pixels, 4×4 pixel binning, and an exposure time of 40 ms. The laser and imaging system were coordinated and triggered using a script programmed into an Arduino board (Arduino Uno R3). During imaging, the mouse's head was fixed to the base using the metal headpiece, and the EEG and EMG

electrodes were connected, while a treadmill allowed the mouse to run freely. For the inflammation and seizure experiments, baseline data were recorded for ~30–60 min, followed by an i.p. injection of either IL-1β (25 μg/kg body weight, to induce inflammation) or kainic acid (10 mg/kg body weight, to induce seizure); data were then recorded for 6 hours. Data from the wide-field imaging, EEG, EMG, running behavior, and infrared video recordings were synchronized using a Power1401 interface (Cambridge Electronic Design) for subsequent analysis.

During data analysis, the seizure-related activity was evaluated through a combination of behavioral observation and electrophysiological recordings using electroencephalography (EEG) and electromyography (EMG). Behavioral seizures were confirmed based on a modified Racine scale.[65] The EEG and EMG (in the neck muscles) electrodes are implanted by surgery. The signal of EEG and EMG were recorded at 1000 Hz, and analyzed by using Spike2 software. Seizure events were confirmed electrophysiologically by the presence of epileptiform discharges on the EEG. These discharges are characterized by high-amplitude, high-frequency spikes and sharp waves, typically with a rhythmic, evolving pattern. The corresponding EMG signal was used to confirm motor involvement during the electrographic seizure. For analyzing the recorded fluorescent images, in order to reduce the artifact from hemodynamic changes, the recorded images were pre-processed using a blood vessel mask to exclude major vascular regions. For analyzing the rise and decay kinetics, the raw $\Delta F/F_0$ traces (1 Hz) were first applied a 5-point moving average smoothing to minimize the impact of high-frequency noise or potential artifacts. The peak response was defined as the maximum amplitude of this smoothed signal. The signal onset was defined as the first time point where the fluorescence signal ($\Delta F/F_0$) exceeded the baseline mean by more than 3 standard deviations (Baseline Mean + 3* SD).The rise t_{50} was calculated as the time interval required for the signal to rise from onset (0%) to 50% of the maximum peak response. The decay t_{50} was calculated as the time interval from the peak response (100%) to the point where the signal decayed by 50% (i.e., returned to 50% of the peak amplitude).

QUANTIFICATION AND STATISTICAL ANALYSIS

In this study, data were analyzed and plotted using Microsoft Excel, Origin Pro, GraphPad Prism, Spike2, or MATLAB. Image data from cultured HEK293T cells and primary neurons were first processed with ImageJ software (NIH), traces were generated by Origin Pro (OriginLab) and pseudocolor images were generated by ImageJ. The fiber-photometry and wide-field imaging data were analyzed using Spike2 and a custom program written in MATLAB. Except where indicated otherwise, all summary data are presented as the mean ± the standard error of the mean (SEM). Data were analyzed using Student's *t* test or one-way ANOVA followed by Tukey's test for multiple comparisons. Where indicated, $^{*}p < 0.05$, $^{**}p < 0.01$, $^{***}p < 0.001$, and n.s., not significant ($p > 0.05$).